

# Mesoporous carbon-confined Au catalysts with superior activity for selective oxidation of glucose to gluconic acid†

Cite this: *Green Chem.*, 2013, **15**, 1035

Chunyan Ma,<sup>a</sup> Wenjuan Xue,<sup>a</sup> Jinjun Li,<sup>a</sup> Wei Xing<sup>\*b</sup> and Zhengping Hao<sup>\*a</sup>

A series of ordered mesoporous carbon (OMC)-supported Au catalysts were successfully prepared by nano-replication, followed by colloidal gold deposition method. Structural analysis showed that the mesopore sizes of the catalysts can be tuned controllably in the range of 3.2–7.6 nm by adjusting the dosage of boric acid used to prepare the carbon supports. TEM observations revealed that the Au nanoparticles were dispersed uniformly in the mesopore channels of the carbon supports. These Au/OMC catalysts were tested for the aerobic oxidation of glucose to produce gluconic acid at 40 °C and pH 9. As demonstrated by the structural analysis and reaction results, the activities of these catalysts were closely related to their mesopore sizes. The catalyst with a mesopore size of 5.4 nm exhibited a superior catalytic activity with a TOF of 4.308 mol<sub>glucose</sub> mol<sub>Au</sub><sup>-1</sup> s<sup>-1</sup> to the catalysts reported previously by other researchers. This high activity was mainly ascribed to its unique structure, consisting of 5.4 nm mesopore channels incorporated with 3.3 nm Au nanoparticles, which facilitates contact between glucose molecules and Au nanoparticles. Besides, the abundant active oxygen species existing on this catalyst surface also promote glucose oxidation.

Received 27th November 2012,  
Accepted 10th February 2013

DOI: 10.1039/c3gc36891b

[www.rsc.org/greenchem](http://www.rsc.org/greenchem)

## 1 Introduction

Over the last two decades, the catalytic transformation of biomass-derived natural resources into valuable compounds has emerged as a technique to minimise pollution.<sup>1</sup> Gluconic acid, resulting from selective oxidation of glucose, is applied as an acidity regulator of food additives and is well suited for use in removing calcareous and rust deposits from metals or other surfaces. In particular, the oxidation of glucose to gluconic acid over noble metal catalysts, including Pt, Pd and Au, has been extensively studied.<sup>2–4</sup> Compared with Pd and Pt catalysts, supported Au catalysts have shown higher catalytic activity with excellent selectivity to gluconic acid as reported.<sup>5–7</sup> Rossi and his co-workers<sup>5</sup> attributed this high catalytic performance to the higher resistivity of Au catalyst to overoxidation and self-poisoning compared to Pt or Pd.

The performance of the supported Au catalyst seems to mainly depend on the size of the Au nanoparticles. Recently, Ishida<sup>8</sup> prepared a series of Au catalysts with excellent catalytic performance for the oxidation of glucose by grinding a volatile dimethyl Au(III)acetylacetonate with various catalyst supports. It was found that the control of the Au particle size is critical in glucose oxidation. Okatsu<sup>9</sup> prepared a variety of Au catalysts with various carbon supports by deposition reduction method. Their results showed that the performance of the catalyst increases with the decrease of the Au nanoparticle size. Ishida<sup>10</sup> deposited Au nanoparticles directly onto cellulose by solid grinding with dimethyl Au(III)acetylacetonate followed by H<sub>2</sub> reduction. The results also demonstrated that the catalyst with smaller Au nanoparticles possesses higher catalytic activity than that with larger Au nanoparticles. As reported by Prüße,<sup>11</sup> the supported Au/Al<sub>2</sub>O<sub>3</sub> catalysts had a long-term stability for the catalytic oxidation of glucose, because the Au nanoparticles did not sinter into larger particles. The previous studies undoubtedly indicated that Au nanoparticles with smaller size (<5 nm) are more catalytically active than those with larger size (>10 nm) in the aerobic oxidation of glucose.

In addition to the particle size, the activity of the Au catalysts seems to be affected by the nature and morphology of the support.<sup>8</sup> Lately, Benkó<sup>12</sup> prepared a series of Au catalysts supported on TiO<sub>2</sub>, SiO<sub>2</sub> and CeO<sub>2</sub> by colloidal gold deposition. Those catalysts showed inferior catalytic performance to the

<sup>a</sup>Department of Environmental Nanomaterials, Research Center for Eco-Environmental Sciences, Chinese Academy of Sciences, Beijing 100085, P. R. China. E-mail: [zpinghao@rcees.ac.cn](mailto:zpinghao@rcees.ac.cn); Tel: +86-10-62923564

<sup>b</sup>School of Science, State Key Laboratory of Heavy Oil Processing, Key Laboratory of Catalysis, China University of Petroleum, Qingdao 266555, P. R. China. E-mail: [xingwei@upc.edu.cn](mailto:xingwei@upc.edu.cn); Tel: +86-533-2788830

†Electronic supplementary information (ESI) available: Small-angle XRD of the OMC supports, nitrogen physisorption isotherms, influence of reaction time on glucose oxidation, XPS Au 4f spectra, IR spectra and O<sub>2</sub>-TPD profiles of some Au/OMC catalysts. See DOI: 10.1039/c3gc36891b

carbon-supported reference catalyst. Al<sub>2</sub>O<sub>3</sub>-supported Au catalysts were also found to be of lower activity than their active carbon-supported counterparts.<sup>4,13,14</sup> Mirescu<sup>15</sup> prepared Au/TiO<sub>2</sub> and Au/C catalysts by the gold sol method, and the former showed lower activity for glucose oxidation than the latter. To date, various active carbon-supported Au catalysts have been tested for the selective oxidation of glucose by many researchers and active carbons are testified to be good supports for Au catalysts. However, Au nanoparticles with uniform size are rarely formed on active carbon due to their wide pore size distribution which provides a heterogeneously steric confinement for Au nucleation and deposition.<sup>16–18</sup> This diversity in Au particle size would inevitably lower the activity and selectivity of the Au catalyst. Besides, the micropores of the active carbons are also blocked easily by Au nanoparticles, which would hinder the diffusion of reactants and products in the pore texture of the active carbons.

Compared with traditional active carbons, ordered mesoporous carbons (OMCs) have such merits as uniform/controlable mesopore size and high surface area, and have been explored as a catalyst support in recent years.<sup>19–21</sup> It has been demonstrated that metal nanoparticles can be dispersed and confined uniformly in the ordered mesopores of OMCs and the mesopore channels of OMCs are not easily blocked by metal nanoparticles, thus exhibiting high catalytic activity.<sup>19</sup> As far as we know, OMC-supported Au catalysts have not yet been reported for the aerobic oxidation of glucose. Herein, OMCs with various pore diameters were prepared by a nano-replication method and used as supports for Au catalysts in glucose oxidation for the first time. The effects of mesopore size and surface chemical nature of the OMCs on glucose oxidation were investigated intensively in this work. It has been demonstrated that the activities of these catalysts were closely related to their mesopore sizes. The catalyst with 5.4 nm mesopores exhibited a superior catalytic activity, with a TOF of 4.308 mol<sub>glucose</sub> mol<sub>Au</sub><sup>-1</sup> s<sup>-1</sup>, compared to the catalysts reported previously by other researchers. This high activity was mainly ascribed to its unique structure: 5.4 nm mesopore channels incorporated with 3.3 nm Au nanoparticles, which facilitates the contact between glucose molecules and Au nanoparticles. Furthermore, the abundant active oxygen species existing on this catalyst surface also promote glucose oxidation. The study of catalysts presented here is critically important for exploring environmentally friendly catalysts with superior activity, and thus high productivity of gluconic acid in mild conditions can be achieved.

## 2 Experimental

### Preparation of ordered mesoporous carbons

(1) **OMC-SBA-100.** The synthesis was performed using sucrose as the carbon source and 2-D hexagonal (*P6mm*) mesoporous silica SBA-15<sup>22</sup> as the hard template according to Ryoo's method.<sup>23</sup> Briefly, 1 g of SBA-15 was mixed homogeneously with 5 ml of aqueous solution containing 0.68 g of

sucrose and 0.07 g of H<sub>2</sub>SO<sub>4</sub> (98 wt%). The amount of sucrose used is expected to just fill up the pores of SBA-15. The resulting sludge was dried at 100 °C for 6 h, and subsequently, 160 °C for another 6 h. Afterwards, the dried sucrose/silica composite was again impregnated with an aqueous solution consisting of 0.4 g sucrose, 0.05 g H<sub>2</sub>SO<sub>4</sub> and 5.0 g H<sub>2</sub>O. The resulting mixture was dried again at 100 and 160 °C. The second sucrose infiltration step aims at completely filling up the pores of SBA-15. The material thus obtained was heated to 900 °C in argon atmosphere. The sucrose was converted to carbon by such a process using sulfuric acid as the catalyst. Finally, the silica framework was removed by dissolution in HF (10 wt%) aqueous solution. The resulting porous carbon material is referred to as OMC-SBA-100.

(2) **OMC-MSU-*x* carbons.** This series of carbons were prepared by a slightly modified Kim's procedure.<sup>24</sup> The procedure is quite similar to the nano-replication method used to prepare OMC-SBA-100, except for the use of MSU mesoporous silica as hard template and a mixture of sucrose and boric acid as the precursor solution. The boric acid content in the precursor solutions was in the range of 2–50 wt% (boric acid/sucrose). Precursor solutions were prepared by adding various amounts of boric acid to a sucrose solution whereby the sucrose concentration was kept constant. The resultant carbons were denoted as OMC-MSU-*x*, where *x* stands for the weight ratio of boric acid to sucrose. A typical procedure for the preparation of OMC-MSU-2 can be described as follows: a precursor solution containing boric acid (0.025 g), sulfuric acid (0.141 g), sucrose (1.25 g), and distilled water (4.0 ml) was allowed to infiltrate the mesopores of 1 g MSU template. The composite material was then dried at 100 °C for 6 h and at 160 °C for 6 h thereafter. The infiltration and drying processes were repeated once more with an additional 3.57 g of precursor solution (66% of first infiltration), before the composite was carbonized at 900 °C for 3 h under argon flow. Finally, the OMC-MSU-2 material was obtained by removal of the inorganic framework using a 10 wt% HF solution.

### Preparation of Au/Meso-C materials

A suitable amount of PVP solution (2 wt%) was added to an aqueous HAuCl<sub>4</sub> solution (0.39 mg Au ml<sup>-1</sup>) under vigorous stirring. Then, a freshly prepared solution of NaBH<sub>4</sub> was slowly added dropwise into the mixture (molar ratio NaBH<sub>4</sub>/Au = 4). The as-prepared mesoporous carbon was added into the mixture afterwards and stirred at room temperature for 2 h, then filtered and washed until no Cl<sup>-</sup> was detected using AgNO<sub>3</sub> solution. After being dried at 70 °C for 5 h, the sample was calcined at 200 °C for 3 h.

**Material characterizations.** Small-angle X-ray diffraction (SAXRD) patterns were recorded on an X'pert PRO powder diffraction system using Cu K $\alpha$  radiation in the 2 $\theta$  range of 0.7–6.0° with a scanning step size of 0.0016°. The textural properties of the samples were measured by N<sub>2</sub> sorption at liquid nitrogen temperature, using a gas adsorption analyzer NOVA 1200. The actual Au content in the samples was determined using an inductively coupled plasma optical emission

spectroscopy (ICP-OES) analyzer (OPTIMA 2000). Before measurements, the solid sample was dissolved in aqua regia. High resolution transmission microscopy (HRTEM) observations were conducted with a JEOL 2011 instrument at an accelerating voltage of 200 kV. The specimens were prepared by ultrasonic dispersion in ethanol, evaporating a drop of the resultant suspension onto a carbon support grid. X-Ray photoelectron spectroscopy (XPS) was conducted on a Kratos Axis Ultra DLD spectrometer with a monochromated Al-K $\alpha$  X-ray source ( $h\nu = 1486.6$  eV), hybrid (magnetic/electrostatic) optics and a multi-channel plate and delay line detector (DLD). All spectra were recorded using an aperture slot of  $300 \times 700$  microns. Survey spectra were recorded with a pass energy of 160 eV and high-resolution spectra with a pass energy of 40 eV. Accurate binding energies ( $\pm 0.1$  eV) were determined with respect to the position of the adventitious C1s peak at 284.8 eV. The Fourier transformed spectroscopy (FT-IR) measurements were performed using a TENSOR 27 infrared spectrometer with a DLaTGS detector. Infrared spectra in the range of  $4000$  to  $400$   $\text{cm}^{-1}$  were obtained by averaging 32 scans with a resolution of  $4$   $\text{cm}^{-1}$  at room temperature. The catalyst powders were mixed with KBr at a mass ratio of 1:2000 and then pressed into thin and transparent slices for analysis. An  $\text{O}_2$  temperature programmed desorption ( $\text{O}_2$ -TPD) test was carried out using a Micromeritics Chemisorb 2720 apparatus. Prior to each TPD run, the catalyst was pretreated with a He flow at  $300$   $^\circ\text{C}$  in a quartz reactor, and the reactor was then allowed to cool to room temperature. The adsorption of  $\text{O}_2$  was measured by exposing the catalyst to a flow of  $\text{O}_2$  for 30 min ( $50$   $\text{ml min}^{-1}$ ). He gas was fed to the reactor at  $50$   $\text{ml min}^{-1}$  for 30 min to purge any residual oxygen. The catalyst was then heated to  $600$   $^\circ\text{C}$  at a constant heating rate of  $10$   $^\circ\text{C min}^{-1}$  under He flow ( $50$   $\text{ml min}^{-1}$ ). The desorption of oxygen was monitored by a TCD detector.

#### Activity measurement of catalysts for glucose oxidation.

Glucose oxidation was carried out at atmospheric pressure by bubbling molecular oxygen ( $100$   $\text{ml min}^{-1}$ ) through the glucose ( $12.39$  g) aqueous solution ( $125$  ml). The catalyst ( $0.25$  g) was added into the glucose solution, and the aqueous dispersion was stirred at  $40$   $^\circ\text{C}$ . The reaction was kept at pH 9 by titrating with  $2.5$  M aqueous NaOH solution. Analysis of the conversion of glucose was performed by HPLC on a Breeze 1525 instrument equipped with a water ( $210$  nm) detector. A Luna Amino C18 column ( $4.6 \times 150$  mm,  $5$   $\mu\text{m}$ ) was used with ethanol and  $1\%$   $\text{H}_3\text{PO}_4$  aqueous solution (9:1) as eluent (flow rate  $1$   $\text{ml min}^{-1}$ ). The product of glucose oxidation was identified as gluconic acid by comparison with the standard compound.

## 3 Results and discussion

### 3.1 The pore structure of Au/OMC catalysts

The as-prepared OMC supports exhibit an ordered 2D hexagonal mesostructure, as can be seen from the XRD patterns shown in Fig. S1.† The XRD patterns exhibit a well resolved

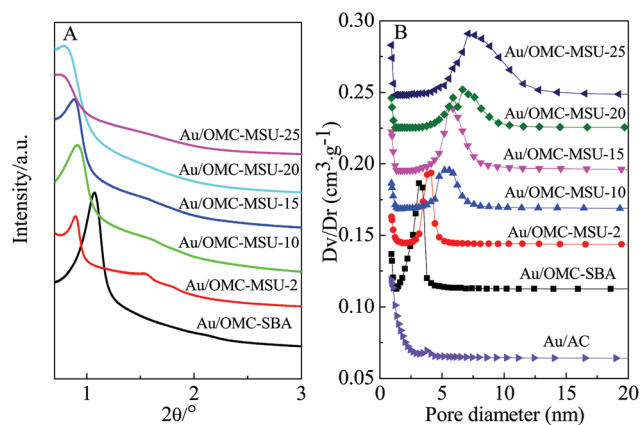


**Fig. 1** (A) Small angle X-ray diffraction of the catalysts and (B) pore size distributions calculated from desorption branch for the catalysts.

peak corresponding to the 100 plane of  $P6mm$  symmetry.<sup>25</sup> For Au/OMC catalysts, they still retain the mesoporous structure well after loading Au particles (as shown in Fig. 1A). The BET surface area and pore structure parameters of these catalysts were determined by  $\text{N}_2$  adsorption and tabulated in Table 1. The as-synthesized Au/OMC catalyst has a mesoporous structure with a high surface area and large pore volume. Nitrogen sorption isotherms (shown in Fig. S2†) indicate that the isotherms of all the Au/OMC catalysts are typical type IV isotherms with large hysteresis loops.<sup>26,27</sup> The capillary condensation partial pressure increases with the ratio of boric acid to sucrose for Au/OMC-MSU samples, indicating the enlargement in mesopore size. The mesopore size distribution (Fig. 1B) confirms the rise of mesopore size with the dosage increase of boric acid. We can also see that the pores of all the Au/OMC catalysts possess a monomodal mesopore distribution and the mesopore diameter of Au/OMC catalysts can be tuned in the range of  $3.2$ – $7.6$  nm by adjusting the ratio of boric acid to sucrose.

### 3.2 Au nanoparticle distributions

During catalyst preparation, the same impregnation procedure was employed in order to obtain Au catalysts with similar loadings and particle sizes, independent of the support used. The total gold loadings on the carbon samples were checked by ICP-OES analysis and the results were listed in Table 1. It was found that the gold loadings are proportional to the pore sizes of the catalysts, which may be due to the fact that large pore size facilitates the deposition of Au nanoparticles onto the carbon pore surface. Actually, there is another clue to account for this phenomenon. It has been reported that the surface oxygen content of the OMC supports is proportional to the boron doping because low-concentration boron doping favors oxygen chemisorptions on the carbon surface. It is also demonstrated by XPS analysis that the surface oxygen contents of OMC-SBA, OMC-MSU-10 and OMC-MSU-15 were  $3.0$ ,  $4.9$  and  $5.7\%$ , respectively. It is well known that the oxygenated groups are typically hydrophilic. Therefore, the prepared

**Table 1** Surface and physical properties and activity of Au/OMC catalysts

Catalyst	N <sub>2</sub> sorption analysis			Supported gold		Activity TOF (s <sup>-1</sup> )
	S <sub>BET</sub> <sup>a</sup> (m <sup>2</sup> g <sup>-1</sup> )	V <sub>t</sub> <sup>b</sup> (cm <sup>3</sup> g <sup>-1</sup> )	D <sub>p</sub> (nm)	Au content <sup>e</sup> (wt%)	S <sub>Au</sub> <sup>f</sup> (nm)	
Au/AC	1115	0.63	2.3 <sup>c</sup>	0.54	3.7	0.343
Au/OMC-SBA	1024	0.92	3.2 <sup>d</sup>	0.60	4.1	1.685
Au/OMC-MSU-2	749	0.93	4.2 <sup>d</sup>	0.62	3.0	2.369
Au/OMC-MSU-10	597	0.84	5.4 <sup>d</sup>	0.65	3.3	4.308
Au/OMC-MSU-15	910	1.35	5.9 <sup>d</sup>	0.69	4.0	1.765
Au/OMC-MSU-20	630	0.97	6.9 <sup>d</sup>	0.70	3.6	1.635
Au/OMC-MSU-25	1170	2.23	7.6 <sup>d</sup>	0.71	3.4	1.513

<sup>a</sup> BET specific surface areas determined from the linear part of the BET equation ( $P/P_0 = 0.05-0.25$ ). <sup>b</sup> Total pore volumes obtained at  $P/P_0 = 0.99$ . <sup>c</sup> Average pore size. <sup>d</sup> Pore size determined from the desorption branch using the BJH method. <sup>e</sup> Obtained by ICP-OES analysis. <sup>f</sup> Mean Au particle size calculated from HRTEM images.

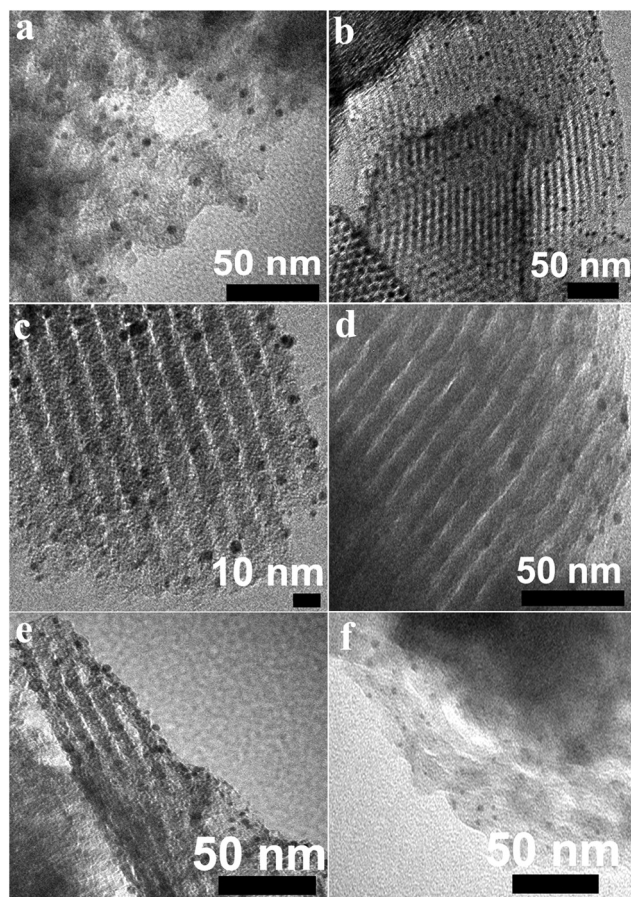


**Fig. 2** HRTEM images of the catalysts. (a) Au/AC; (b) Au/OMC-SBA; (c) Au/OMC-MSU-2; (d) Au/OMC-MSU-10; (e) Au/OMC-MSU-15 and (f) Au/OMC-MSU-25.

carbon supports may show systematically increasing surface hydrophilicity with the increase of the boron doping. Because the  $\text{HAuCl}_4$  aqueous solution as an impregnation precursor is hydrophilic, the carbon support with a more hydrophilic carbon surface has advantages in the infiltration of the Au precursor, thus resulting in higher gold loading.

In order to clearly image the morphological dispersion of Au nanoparticles on carbon supports. HRTEM observations were conducted. It can be seen from Fig. 2 that Au

nanoparticles, imaged as black dots, are presented as pseudo-spherical particles and incorporated uniformly into ordered mesopores of the carbon supports for Au/OMC catalysts. The mean Au particle sizes were also calculated from HRTEM images. It was found that the Au particle sizes are independent of the pore size of the carbon supports (Table 1). The Au particle sizes of all the Au/OMC catalysts were dispersed in a narrow range of 3.0–4.1 nm. Considering that HRTEM instrumental and computational errors existed, such differences in the Au particle sizes of the catalysts investigated can be neglected. It was reported that small Au nanoparticles (*e.g.* less than 5 nm) have a high catalytic activity in glucose oxidation.<sup>8–10</sup> In this regard, all the catalysts as-prepared in this work are expected to be highly active. However, for the Au/AC catalyst, it should be noted that the average pore size of AC is 2.3 nm, which is obviously smaller than the mean size of Au nanoparticles supported on AC. So, it is reasonable to deduce that Au nanoparticles are dispersed on the outer surface of AC support. By contrast, for Au/OMC-MSU catalysts, the pore sizes of the carbon supports are larger than the sizes of Au nanoparticles supported on them. As a result, Au nanoparticles can be dispersed and confined in the mesopore channels of the OMC supports.

In addition to Au loadings and dispersion, the valance of Au nanoparticles was determined by Au4f XPS (Fig. S3<sup>†</sup>). It is reported that the typical binding energies of Au4f<sub>7/2</sub> for Au<sup>0</sup> and Au<sub>2</sub>O<sub>3</sub> are located at 83.8 and 86.3 eV, respectively.<sup>28</sup> In our Au4f XPS measurements, it was found that Au4f binding energies in Au/OMC catalysts are 84.3 eV, located between 83.8 (Au<sup>0</sup>) and 86.3 eV (Au<sub>2</sub>O<sub>3</sub>), suggesting the Au valance is indexed to Au<sup>δ+</sup>, namely Au with a fractional positive charge.

### 3.3 Analysis of surface functionality

Carbon surface chemistry plays an important role in both catalyst dispersion and catalytic activity.<sup>29</sup> The O1s spectra (Fig. 3A) of Au/OMCs can be resolved into four peaks (Fig. 3A).<sup>30,31</sup> The peak at a binding energy of 531–531.9 eV corresponds to the carbonyl oxygen of quinines; the peak at a binding energy of 532.3–532.8 eV corresponds to C=O in esters, anhydrides and phenolic groups; the peak at a binding energy of 533.1–533.8 eV corresponds to C–O in esters and

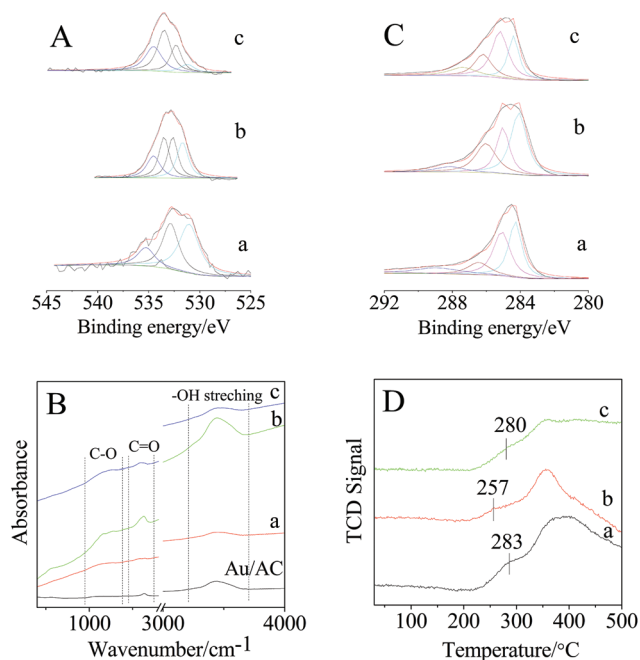


**Fig. 3** (A) XPS O1s spectra, (B) IR spectra, (C) XPS C1s spectra and (D) O<sub>2</sub>-TPD profiles of the Au/OMC catalysts. (a) Au/OMC-SBA; (b) Au/OMC-MSU-10; (c) Au/OMC-MSU-15.

anhydrides, and the peak at a binding energy of 534.3–535.4 eV corresponds to COOH. For Au/OMC-MSU-10, one main peak at 532.6 eV (relative atomic percentage: 26.6%) and another main peak emerged at 533.5 eV (relative atomic percentage: 27.7%) are attributed to C=O and C–O of esters and anhydrides, respectively. Compared to Au/OMC-MSU-10, we observe a decrease of the C–O of esters and anhydrides for Au/OMC-SBA and a decrease of the C=O of esters and anhydrides for Au/OMC-MSU-15. The presence of each functional group was confirmed by FT-IR measurements (shown in Fig. 3B and Fig. S4†). For example, a C–O stretching vibration emerges in the 1000–1260 cm<sup>-1</sup> range, and a C=O stretching vibration in carboxylic acids or isolated carbonyl groups emerges in the 1550–1650 cm<sup>-1</sup> range.<sup>32,33</sup> Fig. 3C shows the evolution of the C1s spectra of Au/OMC catalysts. The C1s peak centered at 284.5 eV is attributed to sp<sup>2</sup>-hybridized graphitic carbon. As for Au/OMC-MSU-10, the intensity of this peak is obviously larger than those of the other catalysts.<sup>34</sup> It could be concluded that the sp<sup>2</sup>-hybridized carbons surrounded with two-oxygen atoms of esters or three-oxygen atoms of anhydrides exist in Au/OMC-MSU-10. There are saturated bond oxygen atoms (C=O) present in the esters and anhydrides. Because there is a lone electron pair existing in sp<sup>2</sup>-hybridized carbon, the O<sup>-</sup> species were formed by electron transfer from carbon to the unsaturated oxygen atoms of esters, and the O<sub>2</sub><sup>-</sup> species were formed by electron transfer from carbon to the double unsaturated oxygen atoms of anhydrides.

The desorption of surface oxygen, such as O<sup>-</sup> and O<sub>2</sub><sup>-</sup> species, was investigated by O<sub>2</sub>-TPD (Fig. 3D and Fig. S5†). The

peak below 300 °C is ascribed to the desorption of surface active oxygen species, such as O<sup>-</sup> and O<sub>2</sub><sup>-</sup>, from the surface of the catalysts,<sup>35</sup> and the desorption peak above 350 °C is attributable to the desorption of oxygen from the oxygen-containing functional groups of carbon. It can be seen that a desorption peak is centered at 257 °C for Au/OMC-MSU-10, which is obviously lower than the peaks of other catalysts. It is obvious that the surface-active oxygen species on the Au/OMC-MSU-10 desorb more easily than the other catalysts. Generally speaking, the easier the surface active oxygen species desorb, the higher the catalytic activity for oxidation reactions.

### 3.4 Catalytic activity

The oxidation of glucose was studied by bubbling oxygen through a 10 wt% aqueous solution of glucose at a flow rate of 100 ml min<sup>-1</sup> at 40 °C and pH 9 in the presence of mesoporous carbon or Au catalysts under ambient pressure. All the ordered mesoporous carbons without gold loading did not exhibit catalytic activity under the same reaction conditions. The activities of glucose oxidation over the supported Au catalysts did not decrease with an extension of reaction time, indicating the good stabilities of these catalysts (Fig. S6†). The selectivities to gluconic acid were very high even above 97%. Thus, the Au nanoparticles were thought to be the active sites for the glucose oxidation. The highest catalytic activity was observed for Au/OMC-MSU-10 with 5.4 nm pore diameter, which showed a TOF of 4.308 mol<sub>glucose</sub> mol<sub>Au</sub><sup>-1</sup> s<sup>-1</sup> at 40 °C and pH 9. It is reported that the TOF over Au/Al<sub>2</sub>O<sub>3</sub> catalysts prepared by incipient wetness method is up to 1.97 mol<sub>glucose</sub> mol<sub>Au</sub><sup>-1</sup> s<sup>-1</sup> at 40 °C and pH 9,<sup>36</sup> and 1% Au/C and 0.5% Au/TiO<sub>2</sub> catalysts showed a TOF of 0.023 and 0.978 mol<sub>glucose</sub> mol<sub>Au</sub><sup>-1</sup> s<sup>-1</sup> at 40 °C and pH 11, respectively.<sup>14</sup> The Au nanoparticles deposited on nanoporous carbon with 2 nm mesopores and hollow cores only showed a TOF of 2.4 mol<sub>glucose</sub> mol<sub>Au</sub><sup>-1</sup> s<sup>-1</sup>.<sup>8</sup> Thus, the activity of Au/OMC-MSU-10 is higher than those reported by other researchers, indicating the high suitability of OMCs as supports of Au nanoparticles, for glucose oxidation to gluconic acid.

The hypotheses for the active states of Au catalysts proposed so far can be classified as follows: (1) specific size of the Au nanoparticles, (2) junction perimeter between gold and the supports and (3) the nature of support.<sup>37</sup> Haruta *et al.*,<sup>8</sup> reported that the metal-oxide-supported Au catalysts showed an increase in TOF with a decrease in Au particle size that appears to be the most dominating parameter in glucose oxidation. However, Comotti *et al.*,<sup>38</sup> reported that the catalytic activity of Au nanoparticles for glucose oxidation was inversely proportional to the Au nanoparticle size in the range of 3–6 nm, but the catalytic activity per gold atom is independent of the Au nanoparticle size. In our work, the TOF of Au/OMC catalysts seems to be independent of the mean Au nanoparticle size (shown in Table 1). The TOF of Au/OMC-MSU-10 is higher than the others, and its mean Au size is smaller than the others, except Au/OMC-MSU-2. The TOF of Au/OMC-MSU-15 is higher than those of Au/AC and Au/OMC-MSU-25 catalysts, but the mean Au nanoparticle size of the former is

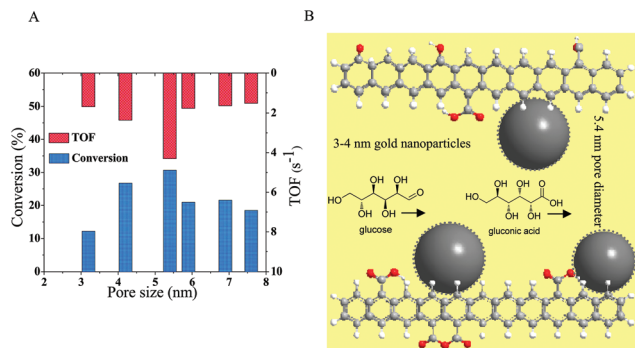


**Fig. 4** (A) The effect of mesopore size on the catalytic activity of the Au/OMC catalysts; reaction conditions: 10 wt% glucose aqueous solution (125 ml),  $O_2$  100 ml  $min^{-1}$ , 40 °C, 6 h; the pH of the solution was kept at 9 by titrating with 2.5 M NaOH. (B) proposed model for the active site of Au/OMC catalysts for the selective oxidation of glucose (light-gray ball: carbon atom; white ball: hydrogen atom; red ball: oxygen atom; dark-gray ball: gold nanoparticles).

also bigger. Therefore, the catalytic activity observed for glucose oxidation over Au catalysts should be influenced more significantly by the nature and structure of the carbon support. As for all the catalysts investigated in this work, it is found that their catalytic activity is closely related to the pore size of the catalyst (Fig. 4A). With the rise in pore size of the catalyst, the TOF value first increases to the upmost value of 4.308  $mol_{glucose} mol_{Au}^{-1} s^{-1}$ , then decreases. Compared to the Au/OMC catalysts, Au/AC shows a much lower TOF value of 0.343  $mol_{glucose} mol_{Au}^{-1} s^{-1}$ . This indicates that mesopore confinement could be an advantageous factor for the catalytic activity of the catalysts. It is demonstrated that either too large or too small a mesopore size deteriorates the catalytic activity of the supported Au nanoparticles. As for the Au/OMC-MSU-10 catalyst, Au nanoparticles with a mean size of 3.3 nm can be well-confined in the mesopore channels with 5.4 nm diameter. In this case, the mesopores of the support were partially occupied by Au nanoparticles but not blocked. It is worthwhile noting that the molecular sizes of glucose and gluconic acid are about  $0.84 \times 0.43 \times 0.29$  nm and  $0.84 \times 0.44 \times 0.29$  nm, respectively, calculated by Gaussian 03. In such a mesoporous carbon supported Au catalyst, therefore, the reactant molecules can diffuse into the mesopores of this catalyst and have sufficient contact with the supported Au nanoparticles, which may be one of the dominating factors accounting for the fast reaction rate on this catalyst.

### 3.5 Active site model for Au/OMC catalysts

The proposed model for the active site of Au/OMC catalysts was shown in Fig. 4B. First of all, the Au nanoparticles were the active sites, as unsupported mesoporous carbons did not show any catalytic activity. Additionally, the supported Au catalysts showed different activities due to the difference of carbon supports. Au/OMC-MSU-10 exhibited the best activity for glucose oxidation among all the catalysts investigated, which was ascribed to the 5.4 nm mesopore channels incorporated with 3.3 nm Au nanoparticles that facilitated the contact

between glucose molecules and Au nanoparticles. Besides, abundant  $O^-$  and  $O_2^-$  species were present on the Au/OMC-MSU-10 surface and desorbed more easily for glucose oxidation, which also contributed to the higher activity of this catalyst.

## 4 Conclusions

In summary, we successfully synthesized a series of ordered mesoporous carbons and deposited Au nanoparticles on the carbon supports. Au nanoparticles with fractional positive charge ( $Au^{\delta+}$ ) were incorporated uniformly in the ordered mesopore channels of the carbon supports. Au/OMC-MSU-10 exhibited a very high catalytic activity with a TOF of 4.308  $mol_{glucose} mol_{Au}^{-1} s^{-1}$  at 40 °C and pH 9. The high catalytic activity of this catalyst can be attributed to two reasons: first, 5.4 nm mesopore channels incorporated with 3.3 nm Au nanoparticles can facilitate the contact between glucose molecules and Au nanoparticles. Second, the abundant active oxygen species present on the catalyst surface promote the catalytic activity for glucose oxidation.

## Acknowledgements

This work is financially supported by the National Natural Science Funds (21107124), the Dean's Award Startup Funds of the Chinese Academy of Sciences, the National Basic Research Program of China (2010CB732300) and the National High Technology Research and Development Program of China (2012AA063101).

## References

- 1 P. Gallezot, *Catal. Today*, 2007, **121**, 76–91.
- 2 A. Abbadi and H. van Bekkum, *Appl. Catal., A*, 1995, **124**, 409–417.
- 3 M. Besson, F. Lahmer, P. Gallezot, P. Fuertes and G. Fléche, *J. Catal.*, 1995, **152**, 116–121.
- 4 C. Baata, N. Decker and U. Prüße, *J. Catal.*, 2008, **258**, 165–169.
- 5 S. Baatz, L. Prati and M. Rossi, *J. Catal.*, 2002, **206**, 242–247.
- 6 A. Mirescu and U. Prüße, *Appl. Catal., B*, 2007, **70**, 644–652.
- 7 S. Hermans and M. Devillers, *Appl. Catal., A*, 2002, **235**, 253–264.
- 8 T. Ishida, N. Kinoshita, H. Okatsu, T. Akita, T. Takei and M. Haruta, *Angew. Chem., Int. Ed.*, 2008, **47**, 9265–9268.
- 9 H. Okatsu, N. Kinoshita, T. Akita, T. Ishida and M. Haruta, *Appl. Catal., A*, 2009, **369**, 8–14.
- 10 T. Ishida, H. Watanabe, T. Bebeko, T. Akita and M. Haruta, *Appl. Catal., A*, 2010, **377**, 42–46.
- 11 U. Prüße, M. Herrmann, C. Baata and N. Decker, *Appl. Catal., A*, 2011, **406**, 89–93.

- 12 T. Benkó, A. Beck, O. Geszti, R. Katona, A. Tungler, K. Frey, L. Guzzi and Z. Schay, *Appl. Catal., A*, 2010, **388**, 31–36.
- 13 C. Baata and U. Prüße, *Catal. Today*, 2007, **122**, 325–329.
- 14 M. Comotti, C. D. Pina, E. Falletta and M. Rossi, *J. Catal.*, 2006, **244**, 122–125.
- 15 A. Mirescu, H. Berndt, A. Martin and U. Prüße, *Appl. Catal., A*, 2007, **317**, 204–209.
- 16 Y. Önal, S. Schimpf and P. Claus, *J. Catal.*, 2004, **223**, 122–133.
- 17 M. Comotti, C. D. Pina, R. Matarrese, M. Rossi and A. Siani, *Appl. Catal., A*, 2005, **291**, 204–209.
- 18 M. Zhang, X. Zhu, X. Liang and Z. Wang, *Catal. Commun.*, 2012, **25**, 92–95.
- 19 T. García, R. Murillo, S. Agouram, A. Dejoz, M. J. Lázaro, L. T. Murciano and B. Solsona, *Chem. Commun.*, 2012, **48**, 5316–5318.
- 20 Y. Zhang, A. Wang and T. Zhang, *Chem. Commun.*, 2010, **46**, 862–864.
- 21 H. Wang, A. Wang, X. Wang and T. Zhang, *Chem. Commun.*, 2008, 2565–2567.
- 22 D. Zhao, J. Feng, Q. Huo, N. Melosh, G. H. Fredrickson and B. F. Chmelka, *Science*, 1998, **279**, 548–552.
- 23 S. Jun, S. H. Joo, R. Ryoo, M. Kruk, M. Jaroniec and Z. Liu, *J. Am. Chem. Soc.*, 2000, **122**, 10712–10713.
- 24 H. I. Lee, J. H. Kim, D. J. You, J. E. Lee, J. M. Kim, W. S. Ahn, C. Pak, S. H. Joo, H. Chang and D. Seung, *Adv. Mater.*, 2008, **20**, 757–762.
- 25 S. Jun, S. H. Joo, R. Ryoo, M. Kruk, M. Jaroniec, Z. Liu, T. Ohsuna and O. Terasaki, *J. Am. Chem. Soc.*, 2000, **122**, 10712–10713.
- 26 K. S. W. Sing, D. H. Everett, R. A. W. Haul, L. Moscou, R. A. Pierotti, J. Rouquerol and T. Siemieniowska, *Pure Appl. Chem.*, 1985, **57**, 603–619.
- 27 M. Kruk and M. Jaroniec, *Chem. Mater.*, 2001, **13**, 3169–3183.
- 28 J. Zhang, Y. Jin, C. Li, Y. Shen, L. Han, Z. Hu, X. Di and Z. Liu, *Appl. Catal., B*, 2009, **91**, 11–20.
- 29 L. Li, Z. H. Zhu, G. Q. Lu, Z. F. Yan and S. Z. Qiao, *Carbon*, 2007, **45**, 11–20.
- 30 I. Kvannd, J. Zhu, T.-J. Zhao, N. Hammer, M. Rønning, S. Raaen, J. C. Walmsley and D. Chen, *J. Phys. Chem. C*, 2010, **114**, 1752–1762.
- 31 P. Brender, R. Gadiou, J.-C. Rietsch, P. Fioux, J. Dentzer, A. Ponche and C. Vix-Guterl, *Anal. Chem.*, 2012, **84**, 2147–2153.
- 32 U. J. Kim, C. A. Furtado, X. Liu, G. Chen and P. C. Eklund, *J. Am. Chem. Soc.*, 2005, **127**, 15437–15445.
- 33 W. Feng, Q. W. Wang, B. Jiang and P. J. Ji, *Ind. Eng. Chem. Res.*, 2011, **50**, 11067–11072.
- 34 S. Kundu, Y. Wang, W. Xia and M. Muhler, *J. Phys. Chem. C*, 2008, **112**, 16869–16878.
- 35 L. Xue, C. Zhang, H. He and Y. Teraoka, *Appl. Catal., B*, 2007, **75**, 167–174.
- 36 C. Baatz and U. Prüße, *J. Catal.*, 2007, **249**, 34–40.
- 37 M. Haruta, *ChemPhysChem*, 2007, **8**, 1911–1913.
- 38 M. Comotti, C. Della Pina, R. Matarrese and M. Rossi, *Angew. Chem., Int. Ed.*, 2004, **43**, 5812–5815.